Physics of the Earth and Planetary Interiors 237 (2014) 51–64

Contents lists available at ScienceDirect

Physics of the Earth and Planetary Interiors

journal homepage: www.elsevier.com/locate/pepi

Thermal and geodynamic contributions to the elevation of the Altiplano–Puna plateau

Claudia Prezzi [a,*], María Paula Iglesia Llanos [a], Hans-Jürgen Götze [b], Sabine Schmidt [b]

[a] CONICET-Universidad de Buenos. Aires. Instituto de Geociencias Básicas, Aplicadas y Ambientales (IGeBA), Fac. de Cs. Exactas y Naturales de la Univ. de Bs. As. Ciudad Universitaria, Pabellón 2, 1428 Buenos Aires, Argentina
[b] Institut für Geowissenschaften, Abteilung Geophysik, Christian Albrechts Universität zu Kiel, Otto-Hahn-Platz 1, 24118 Kiel, Germany

ARTICLE INFO

Article history:
Received 3 September 2013
Received in revised form 10 September 2014
Accepted 1 October 2014
Available online 14 October 2014

Keywords:
Altiplano–Puna
Topography
Thermal isostasy
Geodynamic topography

ABSTRACT

The most remarkable feature of the Central Andes is the Altiplano–Puna plateau. This plateau is characterized by 3.5 km average elevation, approximately 70 km crustal thickness and very high heat flow. The upper mantle structure changes along strike below the plateau. The upper mantle below the Puna becomes hotter, and the lithosphere becomes thinner and weaker. These features suggest that thermal isostasy could play a role in the compensation of the Altiplano–Puna. Thermal isostasy is the geodynamic process whereby regional variations in the lithospheric thermal regime cause changes in elevation. Elevation changes result from variations in rock density in response to thermal expansion. The aim of this study is to estimate the thermal and geodynamic contributions to the elevation. While the thermal component of the Altiplano elevation would be of 1 km, the thermal contribution to the southern Puna elevation would be of 1.5 km. However, in the case of the southern Puna a portion of the actual topography (~20%) cannot be explained considering only compositional and thermal effects, suggesting additional geodynamical support. The obtained results suggest that the thermal state of the lithosphere would play a significant role in the elevation of the Central Andes, and may be responsible of some of the geological differences displayed by the Altiplano and the Puna.

1. Introduction

The most remarkable feature of the Central Andes is the Altiplano–Puna plateau (Fig. 1). This plateau is 300 km wide, 2000 km long, has an average elevation of 3.5 km and a crustal thickness of approximately 70 km (Yuan et al., 2000, 2002; ANCORP-Working-Group, 2003; McGlashan et al., 2008). It is the highest plateau in the world associated with abundant arc magmatism, and is second only to Tibet in height and extent.

The development of the Altiplano–Puna is linked to the subduction of the Nazca plate under the South American plate coupled with simultaneous under-thrusting of the Brazilian Shield. The plateau overlies a 30° east-dipping segment of the Nazca plate; north of 12°S and south of 28°S the subducted plate dips subhorizontally and an internally drained plateau is absent (Jordan et al., 1983; Isacks, 1988). In the region of steep dip, basaltic-andesitic volcanism is active, while recent volcanic activity is not detected to the north and south. Local volcanic edifices are present within the plateau. The volcanic arc (Western Cordillera in Fig. 1) and local volcanic centres have been active from Miocene to present time (Jordan and Gardeweg, 1989).

Due to significant differences along the plateau, it is divided in the Altiplano (north of 22°S) and the Puna (south of 22°S) (Bianchi et al., 2013). The Puna plateau has an average altitude of ~4.2 km above sea level, being approximately 1 km higher than the Altiplano plateau (~3.2 km). This difference in elevation requires an explanation. In general, regional subsidence and uplift are related to one or more of the following mechanisms: (i) dynamic effects of asthenospheric flow, mantle convection and plumes, (ii) flexural response of the lithosphere to loading and (iii) isostatic readjustments (Allen and Allen, 2013).

The main objective of this study is to assess the contribution of density variations within the lithosphere to its isostatic state and surface elevation. It is considered that the actual topography is the sum of compositional effects (related to density structure), thermal effects and geodynamic effects. Several authors noted that the Puna shows lower amount of structural shortening than the Altiplano (e.g. Allmendinger et al., 1997; Gerbault et al., 2005). Shortening values are sufficient to account for crustal cross

* Corresponding author. Tel./fax: +54 11 4788 3439.
E-mail addresses: prezzi@gl.fcen.uba.ar (C. Prezzi), mpiglesia@gl.fcen.uba.ar (M.P. Iglesia Llanos), hajo@geophysik.uni-kiel.de (H.-J. Götze), sabine@geophysik.uni-kiel.de (S. Schmidt).

http://dx.doi.org/10.1016/j.pepi.2014.10.002
0031-9201/

sectional area in the Altiplano north of 22°S, but are less than that needed in the Puna south of 22°S (McQuarrie, 2006). Moreover, the crustal thickness of the Puna is ~60 km, being ~10 km thinner than that of the Altiplano (Yuan et al., 2000; Heit et al., 2008; McGlashan et al., 2008; Wölbern et al., 2009; etc.). Therefore, variations in shortening amount and crustal thickness cannot account for the observed elevation differences between the Puna and the Altiplano if a simple Airy isostatic model is assumed (e.g. Kley and Monaldi, 1998; McQuarrie, 2006).

In addition, along the Puna, strike-slip faults and lineaments are responsible of crustal segmentation. One of such faults, the NW-SE trending Olacapato-Toro Lineament separates the northern Puna (between ~22° and 24°S) from the southern Puna (between ~24° and 28°S); (Bianchi et al., 2013). Conspicuous differences between the northern and southern Puna plateau were previously noted by several authors (e.g. Alonso et al., 1984; Kay et al., 1994, etc.). Since the late Miocene, an ignimbrite "flare-up" has produced a major volcanic province, the Altiplano–Puna Volcanic Complex (APVC); (de Silva, 1989; Zandt et al., 2003). The APVC covers approximately 50,000 km^2 between 21°S and 24°S. Below the Altiplano–northern Puna the existence of a partial melting zone at mid-crustal depth (Altiplano–northern Puna Magma Body) has been established by a number of independent observations (e.g. extreme high electrical conductivity zones, broad low seismic velocity zones, etc.); (e.g. Chmielowski et al., 1999; Yuan et al., 2000; McGlashan et al., 2008; Wölbern et al., 2009). Chmielowski et al. (1999) identified a very low velocity layer at a depth of 19 km, which they interpreted as a regional sill-like magma body associated with the APVC. Yuan et al. (2000) detected an intracrustal low velocity zone below the entire Altiplano–northern Puna. They interpreted it as a zone of continuing metamorphism and partial melting that decouples upper-crustal imbrication from lower-crustal thickening.

Fialko and Pearse (2012) identified on the basis of space geodetic observations the existence of an uplift in the southern Altiplano–northern Puna (22°15′S–67°15′W) at a rate of ~10 mm/year, which persisted over the past two decades and is surrounded by a broad zone of subsidence. These authors proposed that the ongoing uplift and peripheral subsidence ("sombrero uplift") would result from ballooning of a large mid-crustal diapir fed by hot low-viscosity material from the Altiplano–northern Puna Magma Body. Recently, Bianchi et al. (2013) performed a teleseismic P-wave tomography study in the southern Puna. They identified a prominent low-velocity body located in the crust between 26–27.5°S. Bianchi et al. (2013) related the detected velocity anomalies with a mid-crustal back-arc melt zone under the southern Puna: the Southern Puna Magma Body (SPMB). The SPMB could be disconnected from the Altiplano–northern Puna Magma Body (Yuan et al., 2000) and the limit between them could be related to the Olacapato-Toro Lineament (Bianchi et al., 2013).

Interestingly, very high heat flow values characterize this portion of the Andean chain (e.g. Henry and Pollack, 1988; Hamza and Muñoz, 1996; Springer and Förster, 1998). Heat flow on the Altiplano–Puna is widely enhanced (around 100–120 mW/m^2), and although reliable data are sparse and scattered, heat flow in the plateau is likely higher than in the volcanic arc. In addition, based on systematic changes observed in the topography, the flexural rigidity, the seismic attenuation (Q), and the chemistry of back-arc lavas, Whitman et al. (1996) proposed that the upper mantle structure changes along strike below the plateau. They suggested that south of 23°S, the upper mantle below the Puna becomes hotter, and the lithosphere becomes thinner and weaker. Findings from tomographic studies (Heit, 2005; Heit et al., 2008) suggest that the thermal state of the southern Puna (~25.5°S) plateau is different from that of the Altiplano (~21°S), indicating the

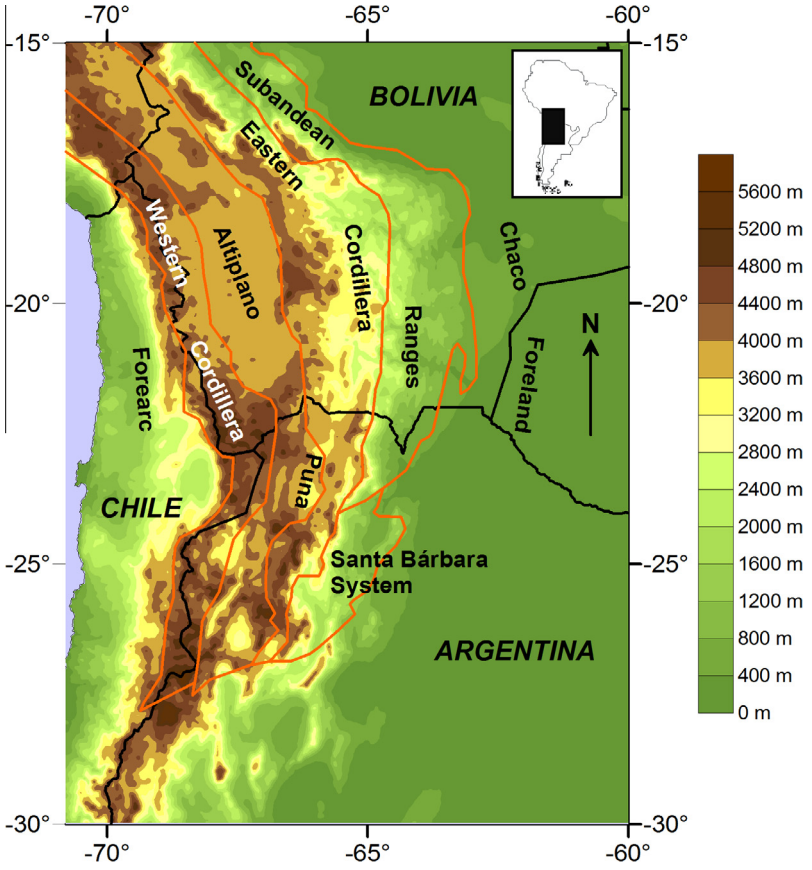

Fig. 1. Topographic map, showing the different morphotectonic units identified in the Central Andes. Inset shows the study area with relation to South America.

presence of colder asthenospheric material beneath the Altiplano and hotter beneath the southern Puna. The tomographic images show low velocity anomalies consistent with asthenospheric material reaching the Moho at 25.5°S (Heit, 2005; Wölbern et al., 2009). Heit (2005) interpreted that such thermal effect could be responsible for the higher elevations of the Puna plateau.

Wölbern et al. (2009) investigated teleseismic data with the receiver function technique detecting a local thinning of the mantle transition zone beneath the southern Puna (~25.5°S), as it would be characteristic for a rising mantle plume. Wölbern et al. (2009) pointed out that due to the poor data coverage, this observation remains to be confirmed by future studies. However, they concluded that a mantle plume could be responsible for the increased heat flow and additional fluid release underneath the southern Puna.

Chulick et al. (2013) presented a new set of contour maps of the seismic structure of South America, based on a large number of new seismic measurements. One striking feature indentified in the crystalline crustal P-wave velocity map is the existence of an east–west band of continental crust between 25° and 30°S, where the data seem to indicate generally low average crystalline velocities (Pcc <6.2 km/s). Regarding the upper mantle, Chulick et al. (2013) observed that under the Andes between approximately 25° and 30°S, upper mantle (Pn) velocities are also low, being less than 8.0 km/s. These authors pointed out that variations in upper mantle velocity largely correlate with the thermal state of the lithosphere, with lower Pn velocities associated with higher lithospheric temperatures. Moreover, the examination of the sub-Moho S-wave (Sn) velocity and Pn maps, indicates a gross similarity with low Sn <4.5 km/s, under the Andes between 25–30°S (Chulick et al., 2013). Histograms of whole-crustal P-wave velocities for South America, are bi-modal, with the lower peak representing crust that appears to be missing a high velocity lower crustal layer. These facts indicate that the southern Puna would be underlain by very low P- and S-wave crustal and upper mantle velocities, along with thinned crust (Chulick et al., 2013).

As shown, many geophysical observations suggest that the thermal state of the lithosphere could play an important role in the isostatic compensation of the Altiplano–Puna. The hypothesis to be tested in this study is that differences in the thermal regime of the lithosphere would cause variations in rock density (due to differential thermal expansion; Hasterok and Chapman, 2007a) and consequently, thermal isostasy would be responsible for the present elevation differences between the Altiplano and Puna.

2. Modelling approach and results

2.1. Thermal isostasy

Thermal isostasy is the geodynamic process whereby regional variations in the lithospheric thermal regime cause changes in elevation. Thereby, elevation changes result from variations in rock density in response to thermal expansion (Hasterok and Chapman, 2007a).

Given two different lithospheric thermal states characterized by a regional geotherm, $T(z)$, and a reference geotherm, $T_{ref}(z)$, we can calculate the corresponding elevation change, $\Delta\varepsilon$th, if we integrate over depth the corresponding temperature differences (Hasterok and Chapman, 2007a):

$$\Delta\varepsilon_{th} = \alpha_v \int_0^{z_{max}} \left[T(z) - T_{ref}(z)\right]\, dz \qquad (1)$$

with α_v being the coefficient of thermal expansion. Considering that both lithospheres have the same adiabat, the maximum depth of integration, z_{max}, is the depth at which the colder geotherm converges to a mantle adiabat.

To calculate regional lithosphere-scale geotherms, we compiled surface heat flow data for the Central Andes, including new values recently published (e.g. Henry and Pollack, 1988; Hamza and Muñoz, 1996; Springer and Förster, 1998; Hamza et al., 2005) (Fig. 2). Table 1 shows surface heat flow data available for the Altiplano–Puna, which range between 70 and 237 mW/m^2. A north–south trending region with heat flow greater than 70 mW/m^2 between 19° and 27°S can be observed (Fig. 2). The forearc in Chile to the west and the Subandean Ranges and foreland basins to the east have lower heat flow (mostly <70 mW/m^2).

The dominant thermal processes in the continental lithosphere are radiogenic heat production and conductive heat transport to the surface (Turcotte and Schubert, 2002). While oceanic geotherms may be identified in terms of age, continental geotherms are mostly expressed in surface heat flow (e.g. Chapman and Pollack, 1977; Turcotte and Schubert, 2002; Hasterok and Chapman, 2007a). To describe lateral variations in the thermal state of continental lithosphere we calculate geotherms as a function of observed values of surface heat flow (Figs. 3a and 4a). To test different scenarios, compare the results and reduce the uncertainties, two different geotherm families are calculated (see Section 2.2).

In order to predict the elevation changes expected for different lithospheric thermal states (Hasterok and Chapman, 2007a), we have to estimate a thermal isostatic curve relating relative elevation to surface heat flow (Figs. 3b and 4b). To calculate this relative elevation, it is necessary to define a reference geotherm. Such reference geotherm corresponds to a surface heat flow of 40 mW/m^2. This lithospheric column with a thermal state represented by the reference geotherm is assigned a surface elevation of 0 km (Hasterok and Chapman, 2007a).

2.2. Geotherm families and corresponding relative elevations due to thermal isostasy

2.2.1. Geotherm family A

We constructed a conductive geotherm family (Fig. 3a) for surface heat flow values (q_0) between 40 and 250 mW/m^2, assuming

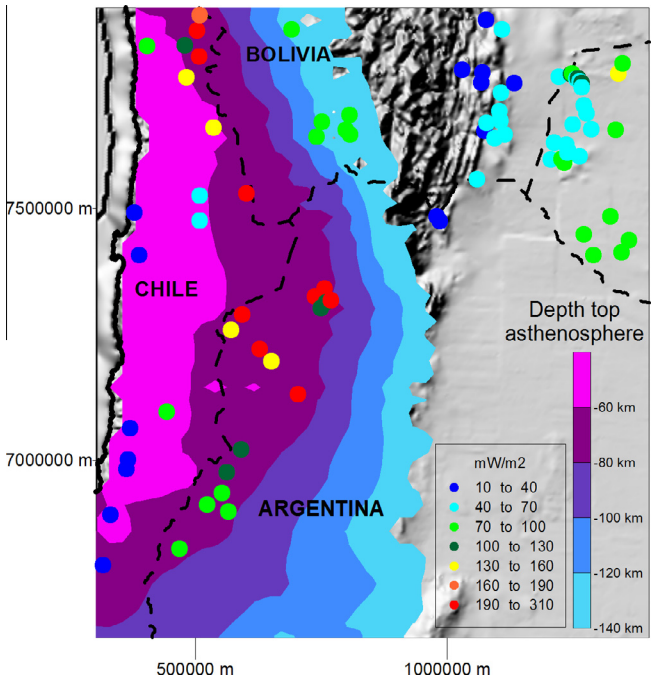

Fig. 2. Surface heat flow data (mW/m^2) and depth to the top of the asthenosphere (km) modelled by Prezzi et al. (2009a) for the Central Andes. Circles: heat flow values, dashed black line: political borders, black line: coast line. UTM projection (−69).

Table 1
Surface heat flow data and the corresponding observed and normalized elevations for the Altiplano–Puna. Latitude: °S; longitude: °W; heat flow: mW/m^2; observed elevation: m; normalized elevation: m.

Latitude	Longitude	Heat flow	Observed elevation	Normalized elevation	Data type	Location	Reference	Certainty
−27.333	−68.37	100	4384.6	1340.8 ± 320.3	Geochemical	Southern Puna–Argentina	Hamza and Muñoz (1996)	Third order
−26.92	−68.083	105	4176.2	879.6 ± 275.9	Geochemical	Southern Puna–Argentina	Hamza and Muñoz (1996)	Third order
−25.92	−66.97	190	5074.1	2086.9 ± 367.3	Geochemical	Southern Puna–Argentina	Hamza and Muñoz (1996)	Third order
−25.333	−67.5	135	3941.1	1581.4 ± 381.1	Geochemical	Southern Puna–Argentina	Hamza and Muñoz (1996)	Third order
−25.12	−67.73	205	3770.7	1299.1 ± 378.1	Geochemical	Southern Puna–Argentina	Hamza and Muñoz (1996)	Third order
−24.37	−66.55	100	4637.4	1616.0 ± 445.1	Geochemical	Southern Puna–Argentina	Hamza and Muñoz (1996)	Third order
−24.27	−66.45	121	4481.6	1644.2 ± 460.5	Geochemical	Southern Puna–Argentina	Hamza and Muñoz (1996)	Third order
−24.23	−66.35	213	4101.9	1506.9 ± 477.4	Geochemical	Southern Puna–Argentina	Hamza and Muñoz (1996)	Third order
−24.17	−66.67	237	4402.8	1481.3 ± 433.9	Geochemical	Southern Puna–Argentina	Hamza and Muñoz (1996)	Third order
−24.017	−66.48	225	4344.1	1738.2 ± 448.3	Geochemical	Southern Puna–Argentina	Hamza and Muñoz (1996)	Third order
−21.3	−66.683	94	3933.1	1676.6 ± 347.6	Conventional	Altiplano-Bolivia	Hamza and Muñoz (1996)	First order
−21.25	−66.05	70	3873.6	721.0 ± 246.6	Conventional	Altiplano-Bolivia	Hamza and Muñoz (1996)	First order
−21.167	−66.133	94	4172.9	854.3 ± 221.3	Conventional	Altiplano-Bolivia	Hamza and Muñoz (1996)	First order
−21.033	−66.583	75	3897.1	1059.6 ± 236.9	Conventional	Altiplano-Bolivia	Hamza and Muñoz (1996)	First order
−20.9	−66.067	70	4128.8	366.8 ± 146.9	Underground mine	Altiplano-Bolivia	Hamza and Muñoz (1996)	Second order
−19.383	−67.183	83	3743.7	1422.9 ± 379.5	Conventional	Altiplano-Bolivia	Hamza and Muñoz (1996)	First order

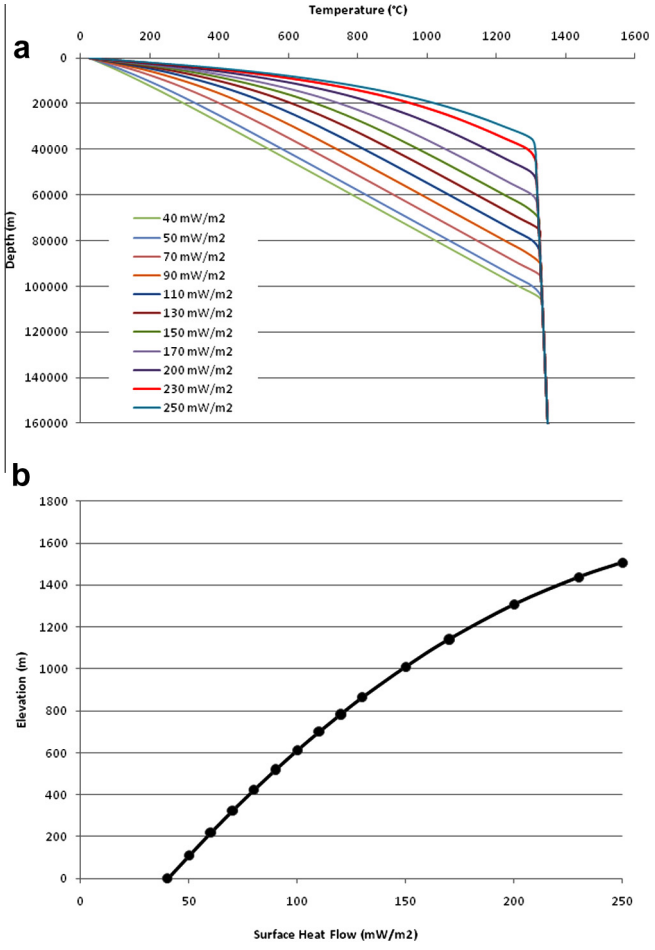

Fig. 3. (a) 1D – steady state conductive geotherm family A for surface heat flow values (q_0) between 40 and 250 mW/m^2. (b) Thermal isostatic relationship showing the predicted thermal elevation for each heat flow value, obtained using the geotherm that corresponds to a surface heat flow of 40 mW/m^2 as reference, and assigning a lithosphere having this thermal state an elevation of 0 km.

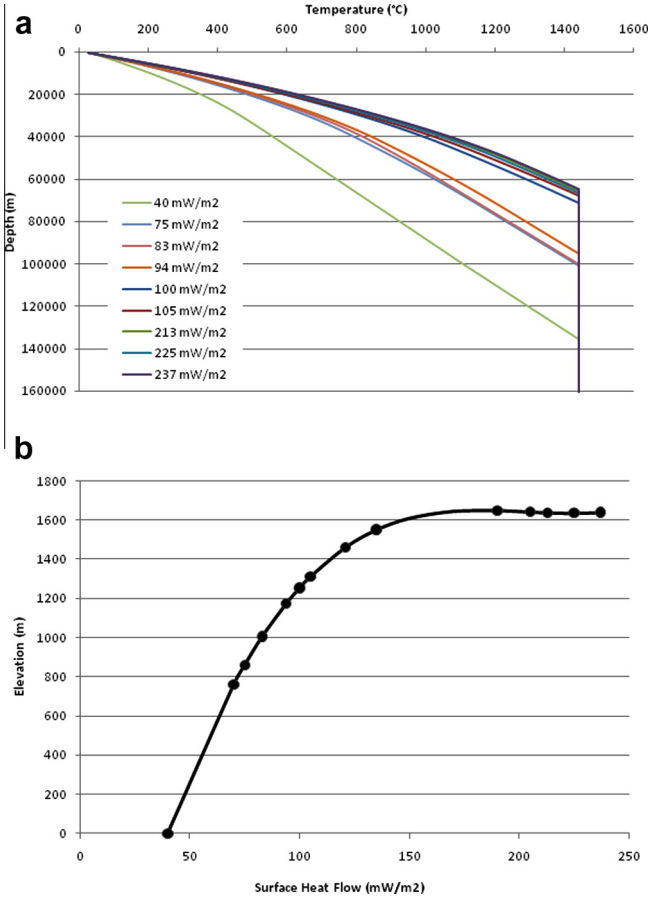

Fig. 4. (a) 1D – steady state conductive geotherm family B for surface heat flow values (q_0) between 40 and 250 mW/m^2. (b) Thermal isostatic relationship showing the predicted thermal elevation for each heat flow value, obtained using the geotherm that corresponds to a surface heat flow of 40 mW/m^2 as reference, and assigning a lithosphere having this thermal state an elevation of 0 km.

1D steady-state temperature conditions, considering exponential decrease of heat production with depth (Turcotte and Schubert, 2002) and a constant thermal conductivity (k) of 2.5 W/mK:

$$T(z) = T_o + \frac{q_m z}{k} + \frac{(q_o - q_m)h_r}{k}(1 - e^{-z/h_r}) \quad (2)$$

where h_r is the length scale for the decrease in radiogenic heat production with depth (10 km) (Turcotte and Schubert, 2002), T_0 is surface temperature (25 °C) and q_m is the mantle (reduced) heat flow to the base of the lithosphere (30 mW/m^2) (Turcotte and Schubert, 2002).

The constant value of thermal conductivity used (k), corresponds to average crustal thermal conductivity reported by

different authors (e.g. Rudnick et al., 1998; Tejero and Ruiz, 2002; Pascal, 2006; Fullea et al., 2007). We also used a mantle adiabat with a potential temperature of 1300 °C and a gradient of 0.30 °C/km (Tassara, 2006; Hasterok and Chapman, 2007a). Using the geotherm that corresponds to a surface heat flow of 40 mW/m^2 as reference, and assigning a lithosphere having this thermal state an elevation of 0 km (Hasterok and Chapman, 2007a), we can predict the thermal contribution to the actual elevation for different surface heat flow data. Fig. 3b depicts the thermal isostatic relationship obtained from Eq. (1) and using a constant coefficient of thermal expansion of 3.0×10^{-05} K^{-1}, consistent with the thermal expansion coefficients of most lithospheric forming rocks (e.g. Roy et al., 1981; Turcotte and Schubert, 2002; Hasterok and Chapman, 2007a). This curve predicts an elevation range resulting from thermal isostasy of 1.5 km.

2.2.2. Geotherm family B

The principal goal of this approach is to derive a geotherm family from a thermal model based on a gravity-constrained 3D density and compositional model (Prezzi et al., 2009a).

We used the Matlab-derived software geothermMOD1.2 (Casini, 2011) to develop the thermal model. GeothermMOD1.2 (Casini, 2011) computes one-dimensional steady-state conductive geotherms involving radiogenic heat production (Fig. 4a). Casini (2011) considered that the most important parameters controlling the variation of temperature with depth in the crust are the heat flow across the Moho, the thermal conductivity and the vertical distribution of heat-producing elements ^{238,235}U, ^{232}Th and ^{40}K. GeothermMOD1.2 software (Casini, 2011) allows setting up models composed of up to five different layers. The user can enter the input parameters directly into editable fields in a simple graphical user interface (GUI): abundances of the heat-producing elements (U, ^{232}Th and ^{40}K), average thermal conductivity, mean density and thickness of each layer. In addition, users can modify the remaining variables of the heat equation (basal heat flow and surface temperature) as required. The temperature at the base of each layer of finite thickness z, characterized by a volumetric heat production rate of A, a thermal conductivity of k, a surface temperature of T_0 and a basal heat flow of q_b is given by:

$$T = -Az^2/2k + (q_b + Az)z/k + T_0 \quad (3)$$

Thickness and density of each layer included in the thermal model were derived from the 3D density model developed by Prezzi et al. (2009a). This 3D density model was constructed using the 3D modelling software IGMAS (“Interactive Gravity and Magnetic Application System”); (Schmidt and Götze, 1999). This modelling algorithm uses triangulated polyhedrons to approximate areas of constant density within the Earth’s crust and mantle. The automated triangulation of model surfaces between parallel vertical cross sections allows the construction of even complicated model geometries (Götze, 1984). This software permits to incorporate additional information such as seismic data (Breunig et al., 2000; Schmidt and Götze, 1999).

The structure of the 3D density model of Prezzi et al. (2009a) considers the existence of upper, middle and lower crust, mantle lithosphere, asthenopheric wedge and asthenosphere (Fig. 5a). In turn, the crust is divided from west to east in different units which represent the Coastal Cordillera, Precordillera, Western Cordillera, Altiplano–Puna, Eastern Cordillera, Subandean Ranges and Chaco (Prezzi and Götze, 2009; Prezzi et al., 2009a, 2011) (Fig. 5a). A partial melting zone at midcrustal depths under the Altiplano–northern Puna and a rheologically strong block beneath the Salar de Atacama basin (Fig. 5a) are included in the model (Prezzi et al., 2009a). The geometry of the modeled bodies is very well constrained by a large amount of additional geophysical and geological data: hypocenter location, reflection and refraction on and offshore seismic lines, travel time and attenuation tomography, receiver function analysis, magnetotelluric studies, thermal models and balanced structural cross sections (e.g. Yuan et al., 2000; Brasse et al., 2002; Schurr and Rietbrock, 2004). The density values assigned to the different bodies forming the model (Fig. 5a) were computed based on documented chemical and/or mineralogical composition (e.g. Lucassen et al., 1999) and information and assumptions about pressure–temperature conditions expected for each body (for details see Prezzi et al., 2009a).

Prezzi et al. (2009a) used 6500 gravity measurements covering an area extending between 19°-30°S and 74°-61°W. The model consists of 31 parallel E-W planes extending between 12°-35°S and 57°-79°W. Trying to reduce the ambiguity and the uncertainty inherent to the gravimetric method, certain aspects of the density structure were not varied during the forward modelling. Thereby, the densities assigned to each modelled body (according to its prevailing lithology; i.e., chemical and mineralogical composition, thereby disregarding temperature effects) were considered fixed and were not changed to obtain a better fit of the measured and calculated anomalies. Likewise, the geometries defined by additional data were not modified. Only those boundaries, of which the geometries were not constrained by other data, were modified.

The forward modelled 3D density structure thoroughly reproduces the measured gravity field. Only less than ~15% of the studied area presents residual anomalies greater than 30×10^{-05} m/s^2 (Prezzi et al., 2009a). Such anomalies are of very short wave length and are not systematically distributed in the map (Fig. 5b). Residual anomaly values are tightly concentrated around 0 m/s^2, with a standard deviation of 16.47×10^{-05} m/s^2. The correlation coefficient between the measured and modelled anomalies is 1 (Prezzi et al., 2009a). These results suggest that the model satisfactorily represents the density structure of the Central Andes.

In our calculation of geotherms we considered the existence of different layers with distinct properties: upper crust, middle crust, lower crust, mantle lithosphere, asthenopheric wedge and asthenosphere. We assumed a surface temperature of 25 °C and a basal heat flow of 30 mW/m^2 for the Altiplano and northern Puna and of 40 mW/m^2 for the southern Puna (Table 2). This difference in basal heat flow is used to match the higher heat flow and the stronger asthenospheric contribution to the thermal budget existent in the southern Puna (Casini, 2011).

Regarding the abundances of heat producing elements, and due to the complete lack of estimates for the studied region, we used the average values proposed by Rudnick and Gao (2003) for the upper crust (^{40}K = 2.8%, U = 2.7 ppm, ^{232}Th = 10.5 ppm), the middle crust (^{40}K = 2.3%, U = 1.3 ppm, ^{232}Th = 6.5 ppm) and the lower crust (^{40}K = 0.61%, U = 0.2 ppm, ^{232}Th = 1.2 ppm). We assumed that there is no sub-crustal heat production (Table 2).

Measured thermal conductivity values are not available for the Central Andes. Hasterok and Chapman (2011) proposed a continental lithosphere heat production model. In their model, these authors estimated P-T-composition dependent thermal conductivities. They assumed a mineralogic composition of the lithosphere, determined by average oxide compositions and common rock types. Their compositional model is equivalent to a granodiorite upper crust (0–16 km), a tonalite middle crust (16–23 km), and a mafic granulite lower crust (23–39 km). Such layer thicknesses and compositions for the crust roughly correspond to the estimates of Rudnick and Gao (2003). Hasterok and Chapman (2011) also assumed average mantle compositions based on garnet xenocryst estimates. They computed thermal conductivities using a P-T-composition dependent model resulting from a combination of lattice and radiative components. According to the values obtained by Hasterok and Chapman (2011), to calculate the geotherms corresponding to heat flow data available in the Altiplano–Puna

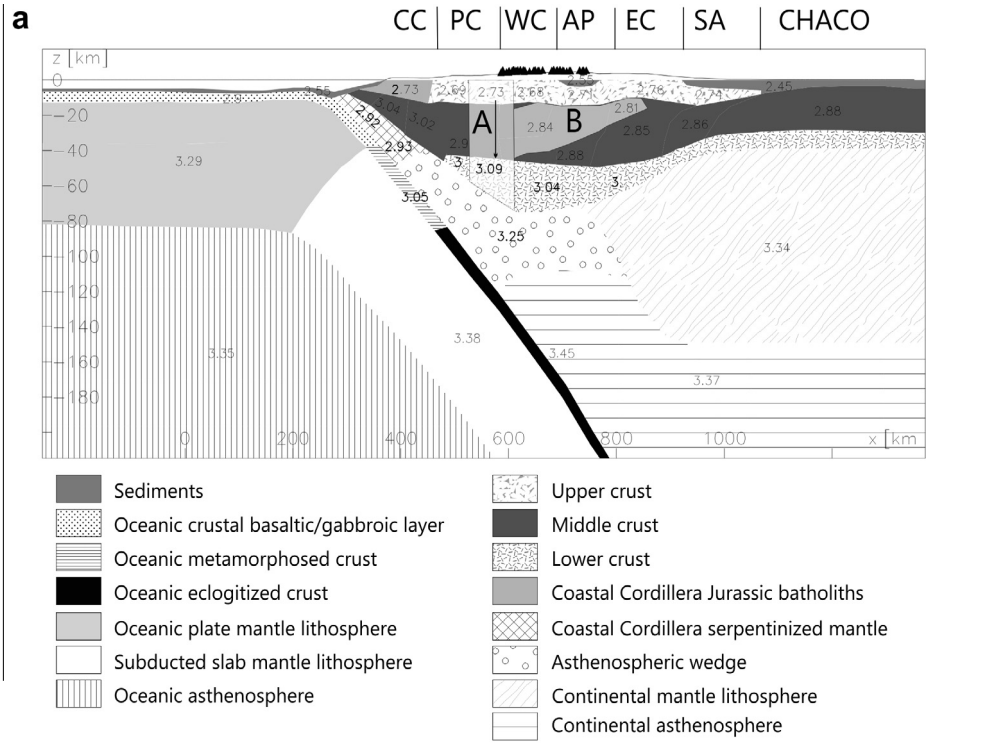

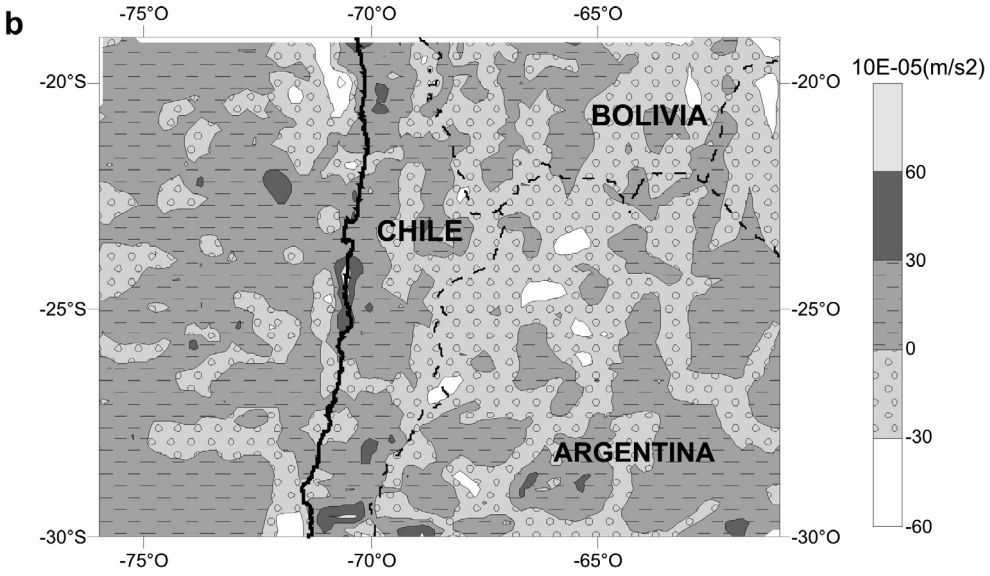

Fig. 5. (a) One of the vertical planes composing the 3D model of Prezzi et al. (2009a) (located at 22°17′S), showing the modeled density structure (density values in Mg/m^3). CC: Coastal Cordillera, PC: Chilean Precordillera, WC: Western Cordillera, AP: Altiplano–Puna, EC: Eastern Cordillera, SA: Subandean Ranges, A: Atacama block, B: Altiplano–Puna partial melting zone. Triangles: position of active volcanoes. (b) Residual Bouguer anomaly generated by the final model of Prezzi et al. (2009a). The residual was calculated as the difference between observed and calculated Bouguer anomaly. Black line: coast line. Dashed black lines: political borders.

(Fig. 2) we used the following average thermal conductivities: 2.3 W/mK for the upper and middle crust, 2.6 W/mK for the lower crust, 2.7 W/mK for the asthenospheric wedge, 2.8 W/mK for the mantle lithosphere and 3.0 W/mK for the asthenosphere (Table 2).

To compute the reference geotherm (which would correspond to a surface heat flow of 40 mW/m^2), we considered the following average thermal conductivities: 3.15 W/mK for the upper crust, 2.5 W/mK for the middle crust, 2.3 W/mK for the lower crust, 3.2 W/mK for the mantle lithosphere and 3.3 W/mK for the asthenosphere (Hasterok and Chapman, 2011) (Table 2). We used thermal conductivity values different from the ones used for the Altiplano–Puna (with surface heat flow of >70 mW/m^2; Table 1) because of the P-T dependency of thermal conductivity (Hasterok and Chapman, 2011).

Geotherms were calculated for each location within the 3D density model at which surface heat flow was measured (Fig. 2, Table 1). We derived the corresponding layer thicknesses and densities from the 3D lithospheric density model (Prezzi et al., 2009a). In the case of the reference geotherm, we used average layer thicknesses and densities corresponding to the Chaco units of the 3D density model. We decided to use these values taking into account that average surface heat flow data for the Chaco is on the order of

Table 2
Parameters used in the calculation of geotherm family B. T_0: surface temperature, Q_b: basal heat flow.

	Heat producing elements abundance			Thermal conductivity (W/m)	T_0 (°C)	Q_b (mW/m^2)
	U (ppm)	Th (ppm)	K (%)			
Altiplano						
Upper crust	2.7	10.5	2.8	2.3	25	30
Middle crust	1.3	6.5	2.3	2.3	25	30
Lower crust	0.2	1.2	0.61	2.6	25	30
Asthenospheric wedge	0	0	0	2.7	25	30
Mantle lithosphere	0	0	0	2.8	25	30
Asthenosphere	0	0	0	3	25	30
Southern Puna						
Upper crust	2.7	10.5	2.8	2.3	25	40
Middle crust	1.3	6.5	2.3	2.3	25	40
Lower crust	0.2	1.2	0.61	2.6	25	40
Asthenospheric wedge	0	0	0	2.7	25	40
Mantle lithosphere	0	0	0	2.8	25	40
Asthenosphere	0	0	0	3	25	40
Reference geotherm						
Upper crust	2.7	10.5	2.8	3.15	25	30
Middle crust	1.3	6.5	2.3	2.5	25	30
Lower crust	0.2	1.2	0.61	2.3	25	30
Mantle lithosphere	0	0	0	3.2	25	30
Asthenosphere	0	0	0	3.3	25	30

40 mW/m^2 (Springer, 1999) (Fig. 2) and average altitude is approximately 200–300 m.

In order to better illustrate the results of these thermal calculations, synthetic wells cutting through the whole lithosphere and showing layer thicknesses, thermal properties, densities, abundances of heat producing elements and calculated temperatures as a function of depth are presented in Fig. 6 for the reference geotherm (q_0 = 40 mW/m^2), one of the Altiplano geotherms (q_0 = 83 mW/m^2) and one of the Southern Puna geotherms (q_0 = 105 mW/m^2).

From this geotherm family we can derive a new thermal isostatic curve (Fig. 4b). Using the geotherm that corresponds to a surface heat flow of 40 mW/m^2 as reference, and assigning a lithosphere having this thermal state an elevation of 0 km (Hasterok and Chapman, 2007a), we can predict the thermal contribution to the actual elevation for different surface heat flow data (Eq. (1) with $\alpha_v = 3.0 \times 10^{-5}$ K^{-1}). It can be observed that the predicted elevation range resulting from thermal isostasy is 1.5 km if we assume a basal heat flow of 30 mW/m^2 for the Altiplano and northern Puna and of 40 mW/m^2 for the southern Puna (Fig. 4b).

2.3. Normalized elevation calculation by isolating compositional effects

The thermal input to continental elevation is difficult to assess, because variations in crustal composition (density) and thickness can mask it. To isolate the thermal component of the actual elevation of the Altiplano–Puna, we need to remove compositional variations involving both crustal thickness and density through an isostatic correction to the observed elevation. This adjustment normalizes any crustal column to a crustal standard (Hasterok and Chapman, 2007a) (Fig. 7). We considered a standard crustal thickness (h_{cst}) of 40 km, a density of the volume above sea level (ρ_t) of 2.67 Mg/m^3 (1 Mg/m^3 = 1 g/cm^3), a standard crustal density (ρ_{cst}) of 2.8 Mg/m^3 and a mantle density (ρ_m) of 3.3 Mg/m^3. It is important to mention that such values are in accordance with the ones estimated by Christensen and Mooney (1995). These authors calculated global continental average crustal thicknesses and densities of 41.5 km and 2.83 Mg/m^3, respectively. Three parameters must be estimated for each studied point to calculate the normalized elevation (ε_{norm}): observed topography (ε_{obs}), "real" crustal thickness (h_c) and "real" crustal density (ρ_c) (Fig. 7).

$$\varepsilon_{norm} = \varepsilon_{obs}\frac{\rho_t}{\rho_m} + h_{cst}\left(1 - \frac{\rho_{cst}}{\rho_m}\right) - h_c\left(1 - \frac{\rho_c}{\rho_m}\right) \quad (4)$$

Observed topography (ε_{obs}) is obtained from the digital elevation model GTOPO30 (U.S. Geological Survey, 1997). "Real" crustal densities (ρ_c) and "real" crustal thicknesses (h_c) and their corresponding confidence intervals, are derived from the above described 3D lithospheric density structure obtained for the Central Andes from 3D forward gravity modeling (Prezzi and Götze, 2009; Prezzi et al., 2009a, 2011).

Thus, "real" crustal thickness (h_c) for each studied point is derived from the corresponding modelled Moho depth. The modelled crust is composed by various bodies with different thicknesses and densities, which represent the upper, middle and lower crust. The total load at a specified depth can be estimated using a function available in IGMAS. From this total load the "real" crustal density (ρ_c) is calculated:

$$\rho_c = \frac{L}{h_c} \equiv \frac{\sum_{i=1}^{N}\rho_i h_i}{h_c} \quad (5)$$

where L is total load, and h_i and ρ_i are the thicknesses and densities of each crustal modelled body along the correspondent vertical column.

The heat flow vs. actual topography plot reveals, that there is no correlation (Fig. 8). In contrast, the normalized elevation shows direct correlation with heat flow as well as a very good fit with the predicted thermal elevations. While the RMS misfit between compositionally normalized elevation and predicted thermal elevation calculated from geotherm family A is of 0.54 km, the RMS misfit between compositionally normalized elevation and predicted thermal elevation calculated from geotherm family B is of 0.30 km. In order to better evaluate the possible existence of differences in the thermal contribution to actual elevation along the Altiplano–Puna, we computed a map of the normalized elevation for the entire studied region from Eq. (4) on a regular grid of 1D lithospheric columns (Fig. 9), using the density structure from the 3D model of Prezzi et al. (2009a). It can be observed that while normalized elevation for most of the Altiplano and northern Puna (north of 24°S) is lower than 1000 m (ranging between 0 and 1000 m), for most of the southern Puna (south of 24°S) it is higher than 1000 m (ranging between 1000 and 1500 m) (Fig. 9).

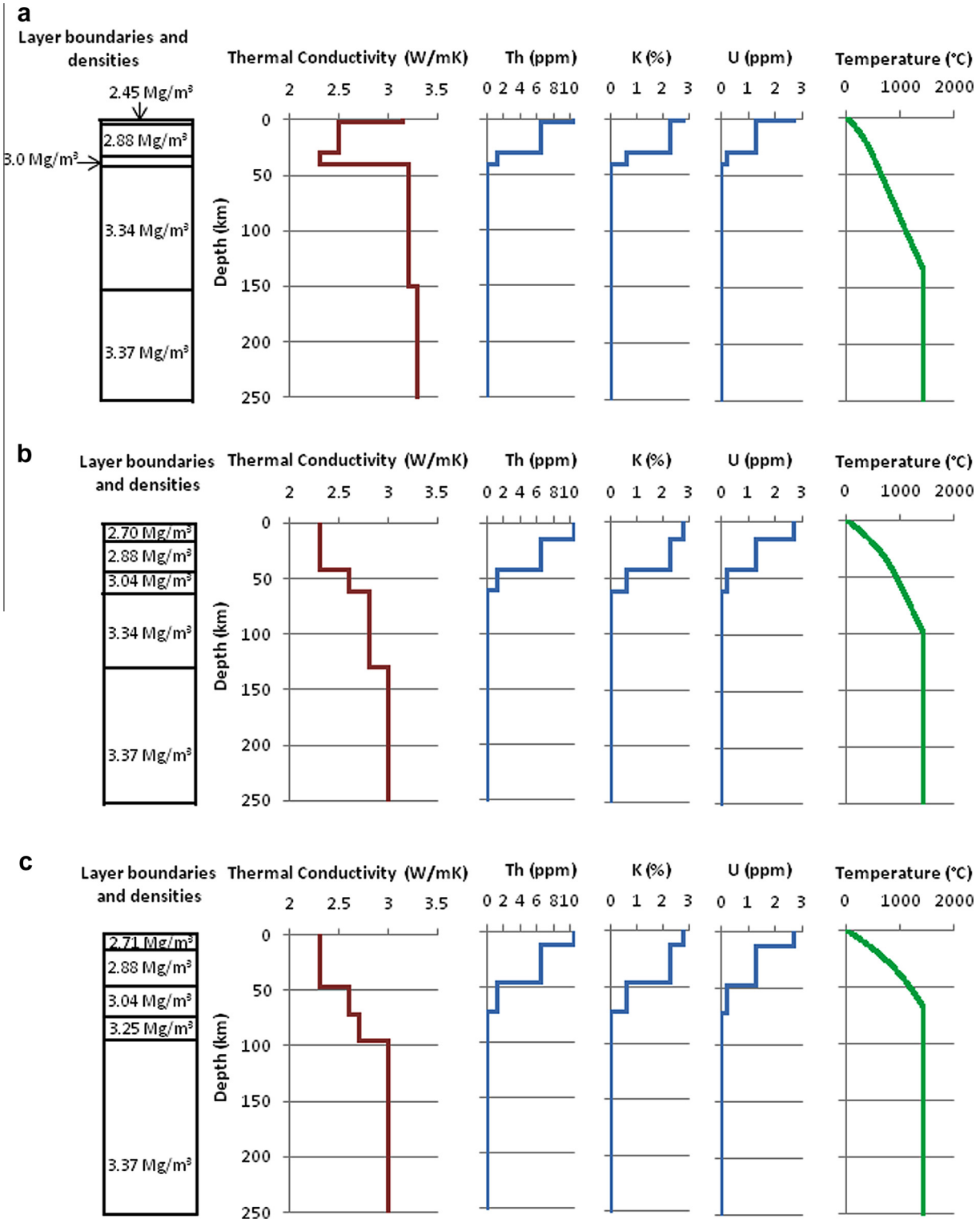

Fig. 6. Synthetic wells cutting through the whole lithosphere and showing layer thicknesses, densities, thermal conductivities, abundances of heat producing elements and calculated temperatures as a function of depth. (a) For the reference geotherm (q_0 = 40 mW/m^2), (b) for one of the Altiplano geotherms (q_0 = 83 mW/m^2) and (c) for one of the Southern Puna geotherms (q_0 = 105 mW/m^2).

2.4. Residual elevation calculation assuming local isostatic (Airy) compensation

If we assume that Airy isostasy applies to the Altiplano–Puna, shortening estimates should explain present surface elevation. However, several authors (e.g. Kley and Monaldi, 1998; McQuarrie, 2006) noted that along the Central Andes there are anomalous regions where the estimates of shortening and thickening cannot account for the observed elevation solely based on Airy isostasy (i.e., regions are not under local isostatic balance). Therefore, we can test if such discrepancies could be elucidated by means of thermal isostasy. To carry out such test we compared

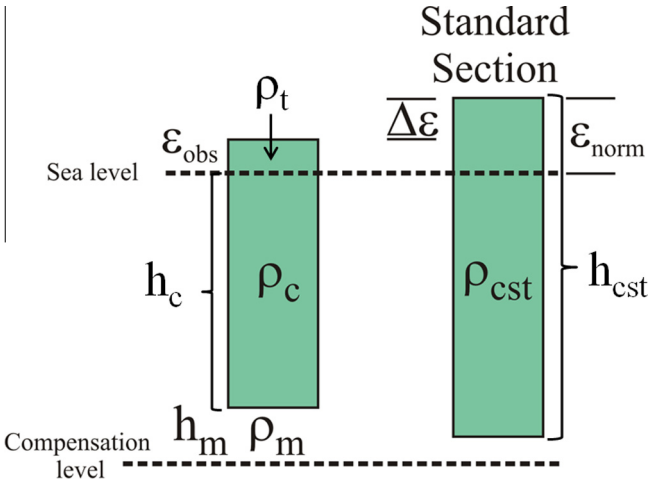

Fig. 7. Cartoon showing the parameters used in the compositional elevation normalization. The observed crustal column (left) is adjusted to a standard crustal section (standard crustal thickness of 40 km and standard crustal density of 2.8 Mg/m^3).

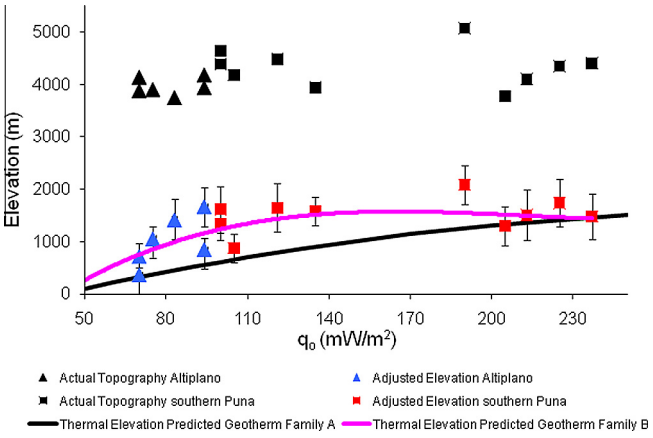

Fig. 8. Actual topography and normalized elevation vs. surface heat flow for the southern Puna (24°–27°S) and the Altiplano (north of 22°S). The thermal contribution to elevation predicted for each heat flow value by the thermal isostatic relationships is also shown (Thermal elevation predicted by geotherm family A, geotherm family B).

the estimated thermal contribution to elevation (normalized elevation: ε_{norm}) with the residual topography (ε_{res}). The residual topography was calculated assuming that the Altiplano–Puna is under local isostatic compensation. We used the Moho geometry and the densities predicted by the 3D gravity model (Prezzi and Götze, 2009; Prezzi et al., 2009a, 2011) to compute the expected topography considering Airy isostasy (Airy topography: ε_{Airy}) (Lliboutry, 1999):

$$\varepsilon_{Airy} = h_{root}\left(\frac{\rho_m - \rho_{root}}{\rho_t}\right) \quad (6)$$

with:

$$h_{root} = h_c - h_{cst} \quad \text{and} \quad \rho_{root} = \frac{L_{root}}{h_c - h_{cst}}$$

where h_{root} is the thickness of the crustal root, ρ_{root} is the density of the crustal root, ρ_t is the density of the volume above sea level (2.67 Mg/m^3) and L_{root} is the load corresponding to the crustal root (Fig. 10). We used the same reference model (h_{cst} = 40 km, ρ_m = of

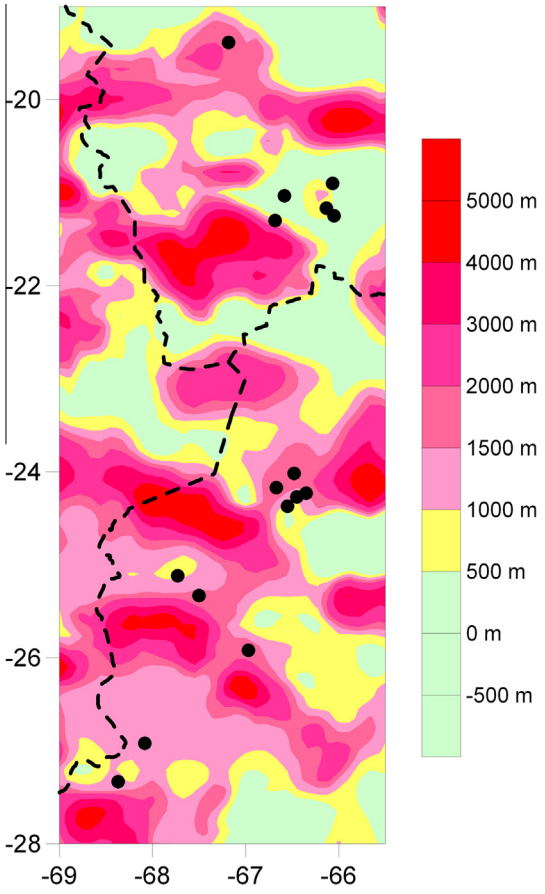

Fig. 9. Map of the normalized elevation for the entire studied region computed from Eq. (4) on a regular grid of 1D lithospheric columns, using the density structure from the 3D model of Prezzi et al. (2009a). Dashed black lines: political borders. Black circles: surface heat flow data used in this study.

3.3 Mg/m^3) as for the calculation of the normalized elevation (Figs. 6 and 10).

Then, we obtained the residual elevation by subtracting Airy topography from actual topography:

$$\varepsilon_{res} = \varepsilon_{obs} - \varepsilon_{airy} \quad (7)$$

Through this calculation, residual elevation (i.e., the fraction of the actual topography that cannot be explained considering Airy compensation) can be compared to the thermal component of elevation (normalized elevation) (Fig. 11).

3. Discussion

3.1. Uncertainties and limitations of the modelling approach

Several authors (e.g. Fukahata and Matsu'ura, 2001; Currie and Hyndman, 2006; Hasterok and Chapman, 2007a) consider that heat flow values higher than ~120–150 mW/m^2 represent the occurrence of nonconductive effects, and filter them out in order to exclude sites affected by advective processes. Hasterok and Chapman (2007a) also state that geotherms calculated for heat flow greater than 120 mW/m^2 lead to widespread melting conditions in the lower crust and upper mantle. Considering that below the Altiplano–Puna the existence of partial melting zones at mid-crustal depth (APMB and SPMB) are well documented, that on the surface an ignimbrite "flare-up" has produced a major volcanic province (APVC), that the upper mantle beneath the southern Puna becomes hotter, and the lithosphere becomes thinner and weaker

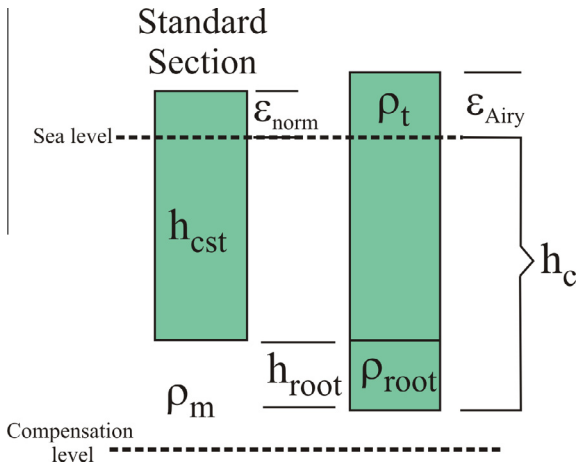

Fig. 10. Cartoon showing the parameters used in the calculation of residual elevation assuming local isostatic (Airy) compensation. ρ_t is the density of the volume above sea level (2.67 Mg/m^3). We used the same reference model (h_{cst} = 40 km, ρ_m = of 3.3 Mg/m^3) as for the calculation of the normalized elevation.

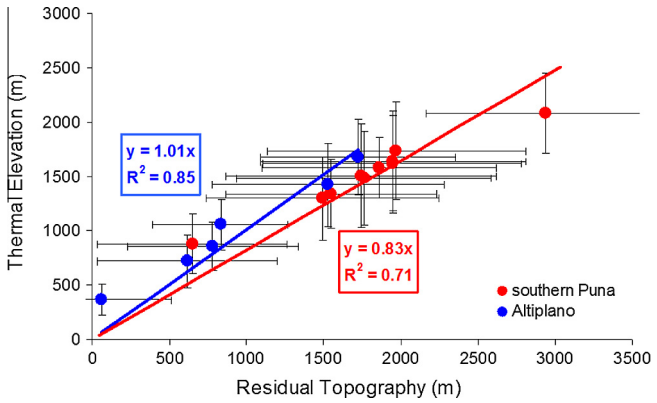

Fig. 11. Residual topography vs. thermal elevation (normalized elevation) for the Altiplano and the southern Puna. The corresponding regression lines are represented: Altiplano: blue continuous line (correlation coefficient 0.85, slope 1.01), Southern Puna: red continuous line (correlation coefficient 0.71, slope 0.83). (For interpretation of the references to colour in this figure legend, the reader is referred to the web version of this article.)

than below the Altiplano (Whitman et al., 1996), and that the possible existence of a mantle plume below the southern Puna (~25.5°S) has been inferred (Wölbern et al., 2009) (see Section 1); we decided not to restrict heat flow values in order to monitor possible differences between the Altiplano and the northern and southern Puna lithospheric thermal states. It is important to remark that in our analysis we do not consider heat flow values measured along the actual magmatic arc, represented by the Western Cordillera (Fig. 1). For this reason, we assume that the observed heat flow values are representative for a larger region and do not reflect only local (magmatic or hydrothermal) effects.

The quality of the surface heat flow data set is variable, consisting of values obtained using conventional methods as well as estimates based on complementary geochemical and underground mine methods (Table 1). Heat flow values by conventional methods represent major parts of the data set for Bolivia, while estimates by geochemical methods constitute almost the whole database for Argentina (Hamza et al., 2005). The limitations imposed by the available data set are obvious, and it is very difficult to set any specific rule concerning the reliability of the calculated heat flow values (Hamza et al., 2005). However, an order of certainty was assigned for the data obtained by different methods. The conventional method is based on direct measurement of the two basic parameters used in heat flow determinations, temperature gradient and thermal conductivity. Originally this method was believed to provide representative values, however a better understanding of the limitations of this methodology induced Hamza and Muñoz (1996) to consider that isolated conventional measurements should be handled with care. In spite of this, first-order certainty was assigned to conventional data in the present work (Table 1).

The underground mine method is one of the oldest used for determining heat flow in underground mines. However, corrections to mine temperature data and to eliminate the disturbing effects of mine ventilation are problematic (Hamza and Muñoz, 1996). Second-order of certainty was assigned to underground mine data in this study (Table 1).

Geochemical methods are often used to obtain a rough estimate of local heat flow at thermo-mineral spring sites. Hamza and Muñoz (1996) remarked that detailed surveys of heat flow patterns have not been carried out in areas of thermal springs on a scale adequate for understanding the local variability of heat flow in the proximity of discharge zones. The main reason is the large cost of drilling the necessary extensive network of deep boreholes. Consequently, the assumption that geochemical methods are "mostly unreliable" is often not based on objective criteria, but on a limited knowledge of the variability of heat flow on a local scale (Hamza and Muñoz, 1996). Local heat flow will be higher in discharge areas than the regional mean. However, overemphasizing this aspect is misleading when the area of the thermal springs is large (Hamza and Muñoz, 1996). Depending on the size of the heat flow pattern under study, "regional" and "local" take on different meanings. It is worthy to note that Hamza and Muñoz (1996) used geochemical data in areas devoid of other data and where the tectonic and geologic context supported a heat flow pattern compatible with the values indicated by this method. Hamza et al. (2005) also pointed out that the geochemical data provide useful constraints for regional trends in areas of poor data density. Particularly, Hamza et al. (2005) noted that in the case of the South America mean heat flow values based on a reduced data set, in which the estimated values by geochemical methods had been eliminated, were representative of regional heat flow in tectonically quiescent areas, which include Pre-cordilleran basins in the west and the Brazilian Platform in the east. On the other hand, the mean values based on the whole data set (including geochemical estimates) were representative of regional heat flow in areas of recent tectonic and magmatic activity, mainly the Andean cordilleran regions. In the present study third-order of certainty was assigned to geochemical data (Table 1).

More sophisticated geotherm models of the continental lithosphere than the ones used in this study are available in the literature (e.g. Chapman, 1986; Chapman et al., 1992), but they require an exhaustive knowledge of several parameters. Considering the limited number of surface heat flow data available, the lack of estimates of the thermal conductivities, heat production and coefficients of thermal expansion of the upper, middle and lower crust and the lithospheric mantle for the Altiplano–Puna, and trying to minimize the uncertainty of our results, we have chosen very simple geothermal models, which are based on the fewest parameters possible.

Moreover, it is not the intention of this study to produce a "best-fitting" thermal model. For such an intention, a much larger surface heat flow or temperature data set would be required, which is not available for the study area. Even so, it should be kept in mind that our calculation of the thermal isostatic relationships involves a number of assumptions. One is that the lithosphere is in thermal equilibrium. However, thermal equilibrium can be lost

easily by a change of the temperature or the heat flow at the bottom of the lithosphere; or by an addition or removal of material from the top through sedimentation or erosion, from the middle through tectonism or from the bottom through convective processes. Particularly, Kay et al., 1994 postulated the occurrence of delamination of the continental lithosphere beneath the southern Puna (~24–27°S) at ~3–2 Ma. This delamination event could indicate that the southern Puna might be in a thermally transient state; however, a transient geotherm can be very difficult to model accurately (Hasterok and Chapman, 2007b). Considering this difficulty, we model the lithospheric geotherms as a steady-state process. Any deviation from the computed steady-state thermal models arising from transient processes will result in a residual elevation that must be taken into account in the interpretations (Hasterok and Chapman, 2007b).

Another assumption is that heat is transported by conduction only. In fact, within the crust there are processes related to hydrothermal systems, regional aquifers, and magmatic systems that can generate heat advection. Magma generation, storage at mid-crustal depths (Altiplano–northern Puna Magma Body; Southern Puna Magma Body) and eruption is well documented in the Puna during Miocene and Pliocene (e.g. de Silva and Gosnold, 2007; Kay and Coira, 2008; Bianchi et al., 2013). De Silva and Gosnold (2007) proposed that the ignimbrite "flare-up" is the record of a crustal scale magmatic system fuelled by a transient spike in mantle power input. These authors carried out numerical simulations using a conductive heat flow model, showing that the presence of the Altiplano–northern Puna Magma Body (APMB) has a significant impact on the thermal state of the crust. De Silva and Gosnold (2007) observed that perturbation of the geotherms after establishment of the APMB reached a maximum after ~5 My, thereafter there is little further change.

The perturbed geotherm modelled by de Silva and Gosnold (2007) shows that temperatures of ~800–1000 °C are reached at ~15–19 km depth. Currie and Hyndman (2006) based on geophysical and petrologic data concluded that the middle crust of the Central Andes is at temperatures of ~800 °C at 20–25 km depth. Hasterok and Chapman (2007a) noted that conductive geotherms calculated for surface heat flow greater than 120 mW/m^2, lead to widespread melting conditions in the lower crust. In our approach, the geotherms constructed for surface heat flow values higher than 150–200 mW/m^2 also show temperatures higher than 800 °C at ~20–25 km depth (Figs. 3a, 4a). These results support the use of conductive geotherms in this work. Therefore, we have chosen to keep our thermal models as simple as possible, interpreting the possible effects of heat advection as residuals from the reference thermal isostatic models. That is to say, any anomalous result is interpreted in terms of properties and processes that differ from the standard models used in this work (Hasterok and Chapman, 2007a). The final assumptions are that the thermal conductivity and the coefficient of thermal expansion are constant with depth. Actually, there is a depth dependence of both parameters.

3.2. Implications of the modelling results

Our results suggest that while the thermal contribution to the actual topography of the Altiplano (north of 22°S) would be of ~1 km, the thermal contribution to the actual topography of the southern Puna (24°–27°S) would be of ~1.5 km (Figs. 8 and 9). Given the scarce number and low quality of the available heat flow data, and the very simple geothermal models used to calculate the thermal isostatic relationships, these values of thermal elevation should be regarded as rough estimates. However, it must be highlighted that the reliability of the compositional adjustment we applied is very high, considering the large number of additional data included in the 3D gravity model of Prezzi et al. (2009a). Thus, these estimates would indicate the existence of first-order geological differences along the Altiplano–Puna.

Shortening values are sufficient to account for crustal cross sectional area in the Altiplano north of 22°S, but are less than that needed in the Puna south of 22°S (McQuarrie, 2006). Our estimates of the thermal contribution to the Altiplano and Puna elevation (Figs. 8 and 9) can indeed explain these features. Furthermore, the 3D gravity model of Prezzi et al. (2009a) shows the presence of thicker lithosphere below the Altiplano than below the Puna (Fig. 2) (Prezzi and Götze, 2009; Prezzi et al., 2009a, 2011). Particularly, the thinnest lithosphere is found below the southern Puna (24–27°S), suggesting a possible relationship between the depth to the top of the asthenosphere and the higher heat flow and the greater thermal contribution to the elevation.

The existence of thinner lithosphere and hotter upper mantle below the southern Puna than below the northern Puna was previously suggested by other authors (e.g. Whitman et al., 1996). Whitman et al. (1996) proposed that such differences in lithospheric thickness result in an Altiplano supported by crustal thickening and a Puna supported by a crustal root and a thermal root.

Moreover, Heit (2005), based on tomographic images, proposed that the Puna plateau would be affected by an anomalous thermal influx from the mantle, caused by the release of fluids from the subducted slab. Heit (2005) pointed out that these thermal anomalies in the asthenosphere would contribute to plateau elevation. Wölbern et al. (2009) presented a receiver function analysis that reveals thinning of the mantle transition zone below the Puna at ~25.5°S. These authors suggested that the detected anomaly might be indicative of the presence of a mantle plume, which could constitute the origin of anomalous temperatures at upper-mantle depths.

Additionally, there are other observations that can be used as indicators of the thermal structure of the uppermost mantle (e.g. Currie and Hyndman, 2006). The effective elastic thickness (Te) inferred from analysis of surface flexure using gravity and topography data, described as the depth to the "brittle-ductile transition", is primarily temperature-controlled (e.g. Hyndman et al., 2009). Hyndman et al. (2009) noted that Te is strongly correlated with surface heat flow in northwestern North America. These authors observed a correlation between thin Te and high upper mantle temperatures and thick Te and low mantle temperatures. Tassara et al. (2007) estimated Te structure of South America using wavelets and satellite-derived gravity data. While Te estimations by Tassara et al. (2007) for the Altiplano and northern Puna (north of ~24°S) range between ~20 and 35 km, for the southern Puna (south of ~24°S) are less than ~15 km.

These facts coincide with and support our results for the southern Puna. Unfortunately, there are no surface heat flow data available for the northern Puna (22–24°S), preventing the evaluation of possible correlations between thermal elevation, asthenospheric depth, the existence of the Altiplano–Puna Magma Body and of the Altiplano–Puna Volcanic Complex.

When we compare the residual topography (ε_{res}) with the thermal component of the elevation (normalized elevation) (ε_{norm}) for the Altiplano (north of 22°S), a very good fit that supports our results is observed (correlation coefficient of 0.85) (Fig. 11). The linear regression parameters (particularly the slope value of 1.01) showed that the residual topography can be completely explained considering only thermal effects. On the other hand, when we compared the residual topography (ε_{res}) with the thermal component of the elevation (normalized elevation) (ε_{norm}) for the southern Puna (24°–27°S), a good fit is observed (correlation coefficient of 0.71) (Fig. 11). However, the linear regression parameters (particularly the slope value of 0.83) showed that a portion of the residual topography (~20%) cannot be explained considering only thermal effects, which is suggestive of additional geodynamic

and/or flexural support. Regarding flexural support, it has been broadly accepted that most of the Altiplano–Puna is locally compensated. Moreover, recent estimates of the Altiplano–Puna elastic thicknesses (e.g. Tassara et al., 2007) range approximately between 0 and 30 km, indicating the existence of weak lithosphere and local compensation.

While tectonics is associated with the isostatic components of topography, the deflections caused by dynamic topography represent the non-isostatic components (Dávila and Lithgow-Bertelloni, 2013). Dávila and Lithgow-Bertelloni, 2013 demonstrated that the Andes and the distal forelands have been mostly uncompensated since the beginning of the Cenozoic and that additional forces, such as mantle downwellings and upwellings, are required to account for the observed topographies in basins and elevations. The Altiplano–Puna plateau has not been studied from this perspective, even when its anomalous low-relief elevation and associated subduction history suggest a complex interaction between mantle dynamics and lithospheric detachment (Dávila and Lithgow-Bertelloni, 2013). Kay et al. (1994) proposed that mechanical delamination of a block (or blocks) of continental lithosphere took place during the late Pliocene below the southern Puna. Between 3 and 0 Ma, Kay and Coira, (2009) documented the occurrence of delamination and the existence of a thick and hot mantle wedge below the southern Puna around 26°S. This delamination event combined with slab steepening (Kay and Coira, 2009), might result in a dynamic topography evolution (Dávila and Lithgow-Bertelloni, 2013).

Gerbault et al. (2005) pointed out that horizontal ductile flow in the lower crust could have occurred along the Central Andes, explaining the observed variations in crustal shortening between the Altiplano and the Puna. Such a mechanism of channel flow may provide geodynamic support to the Altiplano–Puna plateau. Ouimet and Cook (2010) developed a viscous flow model for the Central Andes, highlighting the relationships between slab dip, lower crustal flow, and topography in the Altiplano–Puna. They showed that as the lower crust between 14° and 28°S becomes hot and weak due to steep subduction, increased shortening in the center of the Central Andes drives longitudinal flow of the lower crust along strike to the north and south. Such redistribution of material results in an apparent discrepancy between local crustal volume and surface shortening. Lower crustal flow would exert a fundamental control on the distribution of topography in the Central Andes, and could explain surface uplift in the southern Puna (24°–27°S) (Ouimet and Cook, 2010).

Also, Valera et al. (2011) performed numerical simulations considering different initial setups where delamination could develop. They observed that predicted dynamic topography is very sensitive to changes in the density of the lower orogenic crust, showing surface uplift adjacent to the delaminating lithospheric mantle for models with a low density lower crust, as is the case in the southern Puna (e.g. Prezzi et al., 2009a). On the other hand, the patterns of predicted surface heat flow (over 100 mW/m^2) and isostatic elevation are not affected by changes in the density of the orogenic lower crust (Valera et al., 2011).

In their models, Krystopowicz and Currie (2013) identified two styles of delamination. Weak mantle lithosphere peels away from the crust at a retreating detachment point, whereas strong mantle lithosphere detaches from the crust and slides into the mantle as a coherent slab at a nearly stationary detachment point. Both styles lead to complete removal of orogenic mantle lithosphere but exhibit differences in the evolution of crustal deformation, surface topography and magmatism. In retreating delamination, mantle lithosphere peels away from the crust, producing contemporaneous migration of crustal deformation and surface uplift. During delamination, upwelling mantle and rapid crustal heating may produce magmatism that migrates across the orogen. In stationary delamination, shortening and uplift are confined to one area, but lithosphere is rapidly removed over a wider area, determined by the presence of weak lower crust. Following removal, the full width of the orogen experiences deformation, uplift and crustal heating, which may produce wide-spread magmatism. This style of removal may have occurred in the southern Puna (Kay and Coira, 2009; Krystopowicz and Currie, 2013). The removal of large volumes of dense lithosphere and influx of asthenospheric heat causes a rapid isostatic increase in surface elevation and ignimbrite eruptions (DeCelles et al., 2009), whereby topography becomes an instantaneous response to delamination (Ueda et al., 2012), in coincidence with our results. Moreover, while the Lower-Middle Miocene basins from Altiplano–Puna were interpreted as flexural depocenters (e.g. Prezzi et al., 2009b, 2014), new experiments (Bajolet et al., 2012) suggest that part of their thicknesses could be explained by delamination as well (Dávila and Lithgow-Bertelloni, 2013) .

Thus, the obtained results suggest that the thermal state of the lithosphere would play a significant role in the elevation of the Central Andes, and may be responsible of some of the geological differences displayed by the Altiplano and the Puna. Further advances in the calculation of the thermal and the geodynamic components of elevation can be achieved only with improvements in both the quality and quantity of the heat flow database, and with a more exhaustive knowledge of thermal conductivities, heat production and coefficients of thermal expansion.

The thermal state of the lithosphere can also play a significant role in the topography at other subduction zones. Currie and Hyndman (2006) compiled observational constraints on the thermal structure of circum-Pacific hot back arcs. These authors used independent indicators of temperature, including surface heat flow and radiogenic heat production, mantle seismic velocity from refraction and tomography studies and thermobarometry studies of mantle xenoliths.

Some examples of hot back arcs studied by Currie and Hyndman (2006) are:

1. The northern Cascadia backarc, which presents high surface average heat flow of 75 mW/m^2, low mantle seismic velocities, estimates of high temperatures from peridotite xenolith thermobarometry, presentday widespread sporadic basaltic volcanism, high elevations (1.5–2 km) for a ~35 km backarc crustal thickness, and an effective elastic thickness less than 30 km.
2. The back arc of the southernmost part of the South America subduction zone (south of 35°S), which shows high surface heat flow, lower than average S wave velocities at depths of 60–150 km, average lithospheric thickness of only ~60 km and, sporadic Plio-Quaternary basaltic volcanism.
3. The Kamchatka back arc, which is characterized by high heat flow of ~70 mW/m^2, lower than average P wave velocities at depths of 50–120 km, slow S waves in the upper mantle, and relatively low gravity (modeled using a hot, low-density mantle).
4. The back arc of the Mexico subduction zone, which shows a high average surface heat flow of 72 ± 17 mW/m^2, slower than average P wave velocities at ~100 km depth, slower than average S wave velocities, high surface elevations (1.5–3 km) for a crustal thickness of 35–40 km, and a depth to the base of the lithosphere of less than 70 km.

The elevation of these and other hot back arc zones could be better understood taking into account thermal support in addition to Airy isostasy. Recently, Hyndman and Currie (2011) interpreted the high elevations of the North America Cordillera to be primarily due to the thermal isostasy effect of high temperatures. These

authors explained the Cordillera versus stable area elevation difference of ~1600 m (after correction for crustal thickness and density) by means of temperature differences.

4. Conclusions

(a) This study estimates the compositional contribution to the elevation of the Altiplano–Puna and removes it by an isostatic adjustment, revealing the thermal and geodynamic effects on elevation.
(b) Observed elevation is not correlated with surface heat flow.
(c) Compositionally normalized elevation (calculated based on a databased 3D geological model to reveal thermal isostatic effects) correlates with surface heat flow and shows a good agreement with predictions of thermal isostasy based on calculated geotherms.
(d) While the thermal component of the Altiplano elevation would be of ~1 km, the thermal contribution to the southern Puna elevation would be of ~1.5 km.
(e) Residual elevation (calculated based on the assumption of Airy isostasy and a corresponding crustal root) is closely correlated with the calculated thermal elevation.
(f) For the Altiplano (north of 22°S) the residual topography can be fully explained considering thermal effects solely. On the other hand, for the southern Puna (24°–27°S) a portion of the residual topography (~20%) cannot be explained considering only thermal effects, suggesting additional geodynamic support.
(g) The thermal state of the lithosphere plays a significant role in the elevation of the Central Andes and may be responsible for some of the geological differences displayed by the Altiplano and the Puna.
(h) Further advances in the calculation of the thermal and geodynamic components of elevation can be achieved only with improvements in both the quality and quantity of the heat flow database, and with a more exhaustive knowledge of subsurface temperatures, thermal conductivities, heat production and coefficients of thermal expansion.

Acknowledgements

This research was funded by the Universidad de Buenos Aires (projects UBACyT 20020100100643 and UBACyT 20020110 100064) and by the National Council of Research (CONICET) PIP 11220090100747. We want to thank specially J. Sippel and an anonymous reviewer for their thorough comments, which helped us to greatly improve this manuscript.

References

Allen, P., Allen, J., 2013. Basin analysis: Principles and application to petroleum play assessment. John Wiley & Sons, p. 632.
Allmendinger, R., Jordan, T., Kay, S., Isacks, B., 1997. The evolution of the Altiplano-Puna plateau of the Central Andes. Annu. Rev. Earth Planet. Sci. 25, 39–174.
Alonso, R., Viramonte, J., Gutierrez, R., 1984. Puna Austral. Bases para el subprovincialismo geológico de la Puna Argentina. IX Congreso Geológico Argentino, Bariloche, Actas 1, 43–63.
ANCORP-Working-Group, 2003. Seismic imaging of a convergent continental margin and plateau in the central Andes (Andean Continental Research Project 1996 (ANCORP'96). J. Geophys. Res. 108. http://dx.doi.org/10.1029/2002JB001771.
Bianchi, M., Heit, B., Jakovlev, A., Yuan, X., Kay, S., Sandvol, E., Alonso, R., Coira, B., Brown, L., Kind, R., Comte, D., 2013. Teleseismic tomography of the southern Puna plateau in Argentina and adjacent regions. Tectonophysics 586, 65–83.
Bajolet, F., Galeano, J., Funiciello, F., Moroni, M., Negredo, A. M., Faccena, C., 2012. Continental delamination: Insights from laboratory models, G3, 13, doi: 10.1029/2011GC003896.
Brasse, H., Lezaeta, P., Rath, V., Schwalenberg, K., Soyer, W., Haak, V., 2002. The Bolivian Altiplano conductivity anomaly. J. Geophys. Res. 107. http://dx.doi.org/10.1029/2001JB000391.
Breunig, M., Cremers, A., Götze, H.-J., Seidemann, R., Schmidt, S., Shumilov, S., Siehl, A., 2000. Geologic mapping based on 3D models using an interoperable GIS: GIS. Journal of Spatial Information Decision Making 13, 12–18.
Casini, L., 2011. A MATLAB-derived software (geothermMOD1.2) for one-dimensional thermal modeling, and its application to the Corsica-Sardinia batholith. Comput. Geosci.. http://dx.doi.org/10.1016/j.cageo.2011.10.020.
Chapman, D., 1986. Thermal Gradients in the Continental Crust. In: Dawson, J. et al. (Eds.), The nature of the lower continental crust, 24. Geol. Soc. Spec. Publ., pp. 63–70.
Chapman, D., Pollack, H., 1977. Regional geotherms and lithospheric thickness. Geology 5, 265–268.
Chapman, D., Furlong, K., 1992. Thermal Gradients in the Continental Crust. In: Fountain, D., Arculus, R., Kay, R. (Eds.), Continental Lower Crust, Geotectonis, vol. 23. Elsevier, New York, pp. 179–199.
Chmielowski, J., Zandt, G., Haberland, C., 1999. The central Andean Altiplano-Puna magma body. Geophys. Res. Lett. 26, 783–786.
Christensen, R., Mooney, W., 1995. Seismic velocity structure and composition of the continental crust: A global view. J. Geophys. Res. 100, 9761–9788.
Chulick, G., Detweiler, S., Mooney, W., 2013. Seismic structure of the crust and uppermost mantle of South America and surrounding oceanic basins. J. S. Am. Earth Sci. 42, 260–276.
Currie, C., Hyndman, D., 2006. The thermal structure of subduction zone back arcs. J. Geophys. Res.. http://dx.doi.org/10.1029/2005JB004024.
Dávila, F., Lithgow-Bertelloni, C., 2013. Dynamic topography in South America. J. S. Am. Earth Sci., http://dx.doi.org/10.1016/j.jsames.2012.12.002.
DeCelles, P., Ducea, M., Kapp, P., Zandt, G., 2009. Cyclicity in Cordilleran orogenic systems. Nat. Geosci. 2, 1–7. http://dx.doi.org/10.1038/NGEO0469.
de Silva, S., 1989. Altiplano-Puna volcanic complex of the central Andes. Geology 17, 1102–1106.
de Silva, S., Gosnold, W., 2007. Episodic construction of batholiths: insights from the spatiotemporal development of an ignimbrite flare-up. J. Volcanol. Geoth. Res. 167, 320–335.
Fialko, Y., Pearse, J., 2012. Sombrero uplift above the Altiplano-Puna Magma Body: Evidence of a Ballooning Mid-Crustal Diapir. Science 338, 250–252.
Fullea, J., Fernández, M., Zeyen, H., Vergés, J., 2007. A rapid method to map the crustal and lithospheric thickness using elevation, geoid anomaly and thermal analysis. application to the Gibraltar Arc System, Atlas Mountains and adjacent zones. Tectonophysics 430, 97–117.
Fukahata, Y., Matsu'ura, M., 2001. Correlation between surface heat flow and elevation and its geophysical implication. Geophys. Res. Lett. 28 (14), 2703–2706.
Gerbault, M., Martinod, J., Hérail, G., 2005. Possible orogeny-parallel lower crustal flow and thickening in the Central Andes. Tectonophysics 399, 59–72.
Götze, H.-J., 1984. Über den Einsatz interaktiver Computergraphik im Rahmen 3-dimensionaler Interpretationstechniken in Gravimetrie und Magnetik. Technische Universität Clausthal, Habilitation Schrift.
Hamza, V., Muñoz, M., 1996. Heat flow map of South America. Geothermics 25, 599–646.
Hamza, V., Silva Dias, F., Gomes, A., Delgadilho Terceros, Z., 2005. Numerical and functional representations of regional heat flow in South America. Phys. Earth Planet. Inter. 152, 223–256.
Hasterok, D., Chapman, D., 2007a. Continental thermal isostasy: 1 methods and sensitivity. J. Geophys. Res. 112, B06414. http://dx.doi.org/10.1029/2006JB004663.
Hasterok, D., Chapman, D., 2007b. Continental thermal isostasy: 2 Application to North América. J. Geophys. Res. 112, B06415. http://dx.doi.org/10.1029/2006JB004664.
Hasterok, D., Chapman, D., 2011. Heat production and geotherms for the continental lithosphere. Earth Planet. Sci. Lett. 307, 59–70.
Heit, B., 2005. Teleseismic tomographic images of the Central Andes at 21 and 25.5°S: an inside look at the Altiplano and Puna plateaus, PhD thesis. Freie Universität Berlin. Scientific Technical Report Nr. 06/05, GeoForschungsZentrum, Potsdam, Germany.
Heit, B., Koulakov, I., Asch, G., Yuan, X., Kind, R., Alcozer, I., Tawackoli, S., Wilke, H., 2008. More constraints to determine the seismic structure beneath the Central Andes at 21°S using teleseismic tomography analysis. J. S. Am. Earth Sci. 25, 22–36.
Henry, S., Pollack, H., 1988. Terrestrial heat flow above the Andean subduction zone in Bolivia and Peru. J. Geophys. Res. 93, 15153–15162.
Hyndman, R., Currie, C., Mazzotti, S., Frederiksen, A., 2009. Temperature control of continental lithosphere elastic thickness Te vs Vs. Earth Planet. Sci. Lett. 277, 539–548.
Hyndman, R., Currie, C., 2011. Why is the North America Cordillera high? Hot backarcs, thermal isostasy, and mountain belts. Geology 39, 783–786.
Isacks, B., 1988. Uplift of the Central Andes plateau and bending of the Bolivian Orocline. J. Geophys. Res. 93, 3211–3231.
Jordan, T., Isacks, B., Allmendinger, R., Brewer, J., Ramos, V., Ando, C., 1983. Andean tectonics related to geometry of the subducted Nazca Plate. Geol. Soc. Am. Bull. 94, 341–361.
Jordan, T., Gardeweg, M., 1989. Tectonic Evolution of the Late Cainozoic Central Andes. In: Ben-Avraham, Z. (Ed.), The evolution of the Pacific Ocean margin. Oxford University Press, p. 193.

Kay, S., Coira, B., 2008, Evolución tecto-magmática andina de la Puna norte y sus implicancias en las fajas plegadas y corridas del antepaís (Jujuy), In: Coira, B., Zappettini, E. (Eds.), Geología y Recursos Naturales de la Provincia de Jujuy. Relatorio 17° Congreso Geológico Argentino, pp. 418–430.

Kay, S., Coira, B.L., 2009. Shallowing and Steepening Subduction Zones, Continental Lithospheric Loss, Magmatism, and Crustal Flow under the Central Andean Altiplano-Puna Plateau. In: Kay, S., Ramos, V., Dickinson, W. (Eds.), Backbone of the Americas: shallow subduction, plateau uplift, and ridge and terrane collision, 204. Geological Society of America Memoir, pp. 229–259.

Kay, S., Coira, B., Viramonte, J., 1994. Young mafic back arc volcanic rocks as indicators of continental lithospheric delamination beneath the Argentine Puna plateau, central Andes. J. Geophys. Res. 99 (B12), 24323–24339.

Kley, J., Monaldi, C., 1998. Tectonic shortening and crustal thickness in the Central Andes; how good is the correlation? Geology 26, 723–726.

Krystopowicz, N., Currie, C., 2013. Crustal eclogitization and lithosphere delamination in orogens. Earth Planet. Sci. Lett. 361, 195–207.

Lliboutry, L., 1999, Quantitative Geophysics and Geology, p. 480, Springer-Verlag-Praxis Books in geophysical sciences.

Lucassen, F., Lewerenz, S., Franz, G., Viramonte, J., Mezger, K., 1999. Metamorphism, isotopic ages and composition of lower crustal granulite xenoliths from the Cretaceous Salta Rift, Argentina. Contrib. Miner. Petrol. 134, 325–341.

McGlashan, N., Brown, L., Kay, S., 2008. Crustal thickness in the central Andes from teleseismically recorded depth phase precursors. Geophys. J. Int. 175, 1013–1022.

McQuarrie, N., 2006. Revisiting shortening estimates along the Bolivian orocline: implications of thermal heating, erosion and crustal flow on the development of a high elevation plateau: in Backbone of the Americas Patagonia to Alaska, GSA Specialty Meetings, Abstracts with Programs 2: 86. Mendoza, Argentina.

Ouimet, W., Cook, K., 2010. Building the central Andes through axial lower crustal flow. Tectonics 29. http://dx.doi.org/10.1029/2009TC002460.

Pascal, C., 2006. On the role of heat flow, lithosphere thickness and lithosphere density on gravitational potential stresses. Tectonophysics 425, 83–99.

Prezzi, C., Götze, H.-J., 2009. Estructura litosférica de los Andes Centrales a partir de un modelo gravimétrico 3D, vol. 65(1). Revista de la Asociación Geológica, Argentina, pp. 81–96.

Prezzi, C., Götze, H.-J., Schmidt, S., 2009a. 3D density model of the Central Andes. Phys. Earth Planet. Inter. 177, 217–234. http://dx.doi.org/10.1016/j.pepi.2009.09.004.

Prezzi, C., Uba, C., Götze, J.-H., 2009b. Flexural isostasy in the Bolivian Andes: Chaco foreland basin development. Tectonophysics 474, 526–543. http://dx.doi.org/10.1016/j.tecto.2009.04.037.

Prezzi, C., Götze, H.-J., Schmidt, S., 2011. The Central Andes Lithospheric Structure from 3D Gravity Modeling. In: Salfity, J.A., Marquillas, R.A. (Eds.), Cenozoic geology of the Central Andes of Argentina. SCS Publisher, Salta, pp. 395–410.

Prezzi, C., Uba, C., Götze, J.-H., 2014. Andean foreland evolution and flexure in NW Argentina: Chaco-Paraná basin. Tectonophysics. http://dx.doi.org/10.1016/j.tecto.2014.04.041.

Roy, A., Beck, A., Touloukian, Y., 1981. Thermophysical properties of rocks, in Physical properties of Rocks and Minerals. In: Touloukian, Y., Ho, C. (Eds.), Data ser. Mater. Prop.. McGraw-Hill, St. Louis, Mo, pp. 409–502.

Rudnick, R., Gao, S., 2003. Composition of the Continental Crust. In: Rudnick, R. (Ed.), Treatise On Geochemistry: The crust, vol. 3. Elsevier, pp. 1–64.

Rudnick, R., McDonough, W., O'Connell, R., 1998. Thermal structure, thickness and composition of continental lithosphere. Chem. Geol. 145, 395–411.

Schmidt, S., Götze, H.-J., 1999. Integration of data constraints and potential field modelling - an example from southern Lower Saxony, Germany. Phys. Chem. Earth (A) 24, 191–196.

Schurr, B., Rietbrock, A., 2004. Deep seismic structure of the Atacama basin, northern Chile. Geophys. Res. Lett. 31. http://dx.doi.org/10.1029/2004GL019796.

Springer, M., 1999. Interpretation of heat-flow density in the Central Andes. Tectonophysics 306, 377–395.

Springer, M., Förster, A., 1998. Heat-flow density across the central Andean subduction zone. Tectonophysics 291, 123–139.

Tassara, A., 2006. Factors controlling the crustal density structure underneath active continental margins with implications for their evolution. Geochem. Geophys. Geosyst. 7. http://dx.doi.org/10.1029/2005GC001040.

Tassara, A., Swain, C., Hackney, R., Kirby, J., 2007. Elastic thickness structure of South America estimated using wavelets and satellite-derived gravity data. Earth Planet. Sci. Lett. 253, 17–36.

Tejero, R., Ruiz, J., 2002. Thermal and mechanical structure of the central Iberian Peninsula lithosphere. Tectonophysics 350, 49–62.

Turcotte, D., Schubert, G., 2002. Geodynamics Cambridge University Press, New York.

Ueda, K., Gerya, T., Burg, J., 2012. Delamination in collisional orogens: Thermomechanical modeling. J. Geophys. Res. 117. http://dx.doi.org/10.1029/2012JB009144.

Valera, J., Negredo, A., Jiménez-Munt, I., 2011. Deep and near-surface consequences of root removal by asymmetric continental delamination. Tectonophysics 502, 257–265.

Whitman, D., Isacks, B., Kay, S., 1996. Lithospheric structure and along-strike segmentation of the Central Andean Plateau: seismic Q, magmatism, flexure, topography and tectonics. Tectonophysics 259, 29–40.

Wölbern, I., Heit, B., Yuan, X., Asch, G., Kind, R., Viramonte, J., Tawackoli, S., Wilke, H., 2009. Receiver function images from the Moho and the slab beneath the Altiplano and Puna plateaus in the Central Andes. Geophys. J. Int. 177, 296–308.

Yuan, X., Sobolev, S., Kind, R., Oncken, O.Andes Working Group, 2000. Subduction and collision processes in the Central Andes constrained by converted seismic phases. Nature 408, 958–961.

Yuan, X., Sobolev, S., Kind, R., 2002. Moho topography in the central Andes and its geodynamic implications. Earth Planet. Sci. Lett. 199, 389–402.

Zandt, G., Leidig, M., Chmielowski, J., Baumont, D., Yuan, X., 2003. Seismic detection and characterization of the Altiplano-Puna magma body, central Andes. Pure Appl. Geophys. 160, 789–807.